Polyhedron 113 (2016) 5–15

Contents lists available at ScienceDirect

Polyhedron

journal homepage: www.elsevier.com/locate/poly

Catechol oxidase mimetic activity of copper(I) complexes of 3,5-dimethyl pyrazole derivatives: Coordination behavior, X-ray crystallography and electrochemical study

Ananyakumari Santra [a,1], Gopinath Mondal [a,1], Moumita Acharjya [a], Pradip Bera [a], Anangamohan Panja [a], Tarun K. Mandal [b], Partha Mitra [c], Pulakesh Bera [a,*]

[a] Department of Chemistry, Panskura Banamali College, Vidyasagar University, Midnapore (E), West Bengal 721152, India
[b] Department of Biotechnology, Haldia Institute of Technology, Hatiberia, Haldia, West Bengal 721 657, India
[c] Department of Inorganic Chemistry, Indian Association for the Cultivation of Science, Kolkata, West Bengal 700032, India

ARTICLE INFO

Article history:
Received 19 February 2016
Accepted 29 March 2016
Available online 13 April 2016

Keywords:
Copper(I) pyrazolyl complex
Catecholase activity
X-ray Crystallography
DFT
Cyclovoltammetry

ABSTRACT

N^1-substituted 3,5-dimethylpyrazole (dmpz) namely, methyl-3,5-dimethyl pyrazole-1-dithioate (L^1) and benzyl-3,5-dimethyl-pyrazole-1-dithioate (L^2) were reacted with zinc(II), copper(II) and cadmium(II) chloride to study their coordination behavior. Ligands L^1 and L^2 produced isostructural complexes with composition $[Cu^I(L^1)_2][Cu^ICl_2]$ (**1**) and $[Cu^I(L^2)_2][Cu^ICl_2]$ (**2**), respectively when reacted with $CuCl_2{\cdot}2H_2O$. Copper (I) (d^{10} system) analogues, **1** and **2**, exhibit prominent catechol oxidase activity in which a nice correlation-the easily oxidizable copper(I) center favoring the oxidation of 3,5-DTBC (3,5-ditertiary butyl catechol) is observed. Most importantly, these two compounds represent the class of copper(I) compounds that are rarely employed for the study of catecholase activity. The kinetics study exhibits a deuterium kinetic isotope effect in the catalytic oxidation of 3,5-DTBC by O_2 as evidenced by about 1.9 times rate retardation in the deuterated solvent, suggesting the hydrogen atom transfer in the rate-determining step from the substrate hydroxy group to the metal-bound superoxo species. With other d^{10} cations, zinc(II) and cadmium(II) the ligand $L^1$and/or L^2 undergoes dissociation into parent pyrazole unit i.e., 3,5-dimethylpyrazole (dmpz) during formation of a monomeric tetrahedral $Zn(dmpz)_2Cl_2$ (**3**) complex and a helical 1-D polymeric chain, $[Cd(dmpz)_2Cl_2]_n$(**4**). The possible role of intramolecular hydrogen-bonding induced helicity has been explored in **4**.

1. Introduction

Several di- and polynuclear copper complexes have been reported in order to understand the active site geometric and electronic structures and to mimic the catalytic reactivity [1–9]. As the met form of catechol oxidase contains Cu^{II}, thus most of the models are reported to be Cu^{II}-based complexes [10–18]. It is now well known that in the catalytic cycle Cu^{II} is reduced to Cu^I with concomitant oxidation of catechol and reoxidation of Cu^I by molecular oxygen regenerates Cu^{II} [13]. However, literature survey reveals that Cu^I-complexes have rarely been employed for mimicking the function of catechol oxidase [18]. The reason may be due to lack of proper structural organization between metal and donor ligand with respect to Cu(II)–Cu(I) redox behavior during alcohol oxidation. In this context pyrazole derived ligands might be a potential chelate to form stable Cu(I) complexes with mimetic catecholate oxidation. Pyrazole being isomeric with imidazole, which is an integral part of biological system, is considered to be the most flexible ligand in coordination chemistry due to its diatopic nature and the coordination flexibility of pyrazolido ion [19,20]. The ease of synthesis of pyrazolyl ligands, varieties of coordination modes with fascinating chemistry, and isomeric structure to imidazole that present in proteins, are the reasons for broad and intensive studies of pyrazole derived compounds. The rich chemistry of pyrazole and their derivatives is attributed to the several chemical merit points such as the presence of localized lone pair of electron on an in-plane orbital and the presence of low energy anti bonding vacant π^* orbitals of the aromatic system guaranteed their π-acidity. The five member pyrazole ring is an important example of π-acid ligand showing σ-donor ability along with π-acceptor capacity. Pyrazole is a weak acid comparable to aliphatic alcohols, and is also weaker base than pyridine or simple aromatic amines.

* Corresponding author.
E-mail address: pbera.pbc.chem@gmail.com (P. Bera).
[1] Ananyakumari Santra and Gopinath Mondal equally contribute to the work.

http://dx.doi.org/10.1016/j.poly.2016.03.055
0277-5387/

The alkylation or arylation of the pyrazole ring changes these values by no more than ±2 pK_a units (the acid pK_a = 14.2 and basic pK_a = 2.5) [21,22]. Further, planarity of the heterocycles ascertained their fewer encumbrances to the coordination sphere during complexation. Besides these the presence of substituent(s) in the pyrazole ring in N^1 or 3(5) positions may vary the steric profile and redox environment of the coordination system. The increasing demands of huge pyrazole based pharmaceutical drugs and catalytic promiscuity of its metal complexes [23] spirited us to continue the research on pyrazole based compounds. The present study includes the interaction of two pyrazole based ligands with d^{10} metal ions e.g., Cu(I), Zn(II) and Cd(II) emphasizing the stereo chemical changes in the formation of coordination compounds. Among the essential elements, copper plays crucial role to all organisms living strictly in aerobic environments. It is present in the active sites of several metalloenzymes and metalloproteins [24,25]. Many copper proteins/enzymes activate molecular oxygen, and the functions of these proteins are of oxygen carriers (hemocyanin) [26] or as catalysts in oxygenation (oxygenases) or oxidation (oxidases) [27] reactions. One of the major enzymes that utilizes molecular dioxygen is catechol oxidase [28], a member of type-3 copper proteins, which catalyzes exclusively the oxidation of a wide range of *o*-diphenols (catechols) to the corresponding *o*-quinones through the four-electron reduction of molecular oxygen to water in a process known as catecholase activity [29–31]. Quinones are highly reactive intermediates that undergo autopolymerization to produce a brown pigment namely melanin, a natural antiseptic, which helps to protect damaged plants against both bacterial and fungal diseases [32]. The met state of catechol oxidase consists of two Cu^{II} centers, each copper is coordinated to three imidazole groups from histidyl residues and joined by a bridging OH [28,33]. Isoelectronic metal systems e.g., Cd(II), Zn(II) are also studied simultaneously with the same set of ligands to compare the structure and activity. The present work emphasize on the effect of substitution on N^1 of 3,5-dimethyl pyrazole (dmpz) in the solid state isolation of coordination compounds with d^{10} metal ions to look insight the structure and activity relationship. The ligands methyl-3,5-dimethyl pyrazole-1-dithioate (L^1), benzyl-3,5-dimethyl-pyrazole-1-dithioate (L^2) and complex **1**, $[Cu^I(L^1)_2][Cu^ICl_2]$, were obtained following the methods described in the previous works [34,36]. Herein, we report for the first time the isolation and structural characterization of three d^{10} complexes $[Cu^I(L^2)_2][Cu^ICl_2]$ (**2**), $Zn(dmpz)_2Cl_2$ (**3**) and $[Cd(dmpz)_2Cl_2]_n$ (**4**) and the catecholase activity of **2** along with analogous complex **1** with detailed kinetics investigations has also been explored.

2. Experimental

2.1. Materials and methods

$CuCl_2{\cdot}2H_2O$, $CdCl_2{\cdot}H_2O$, $ZnCl_2$, DMSO and CS_2 were reagent grade, commercial products of MERCK and were used without further purification. Reagent grade benzyl chloride and methyl iodide were purchased from Spectrochem chemical company. Analytical grade, methanol, ethylene diamine and ethylene glycol were purchased from Himedia chemical company and used without further purification. Solvent ethanol (Changshu Yangyuan Chemical, China) was dried and distilled before use. Ligand L^1, L^2 and complex **1** were synthesized following earlier methods [34–36].

2.2. Synthesis of $[Cu(L^2)_2]$ $[CuCl_2]$ (**2**)

$CuCl_2{\cdot}2H_2O$ (10 mmol, 1.70 g) dissolved in 20 mL of ethanol is added drop wise to the acetonitrile solution of L^2 (10 mmol, 2.62 g) with constant stirring. Stirring is continued for another half an hour where a deep blue colored compound separated out. The precipitate formed was filtered, washed with excess ethanol and dried in an oven at 90 °C. Yield: 80%, Mass spectrum *m*/*z* value: 587 (molecular ion peak for $Cu^I(L^2)_2^+$). *Anal.* Calc. for $C_{26}H_{28}Cl_2Cu_2N_4S_4$: C, 43.20; H, 3.90; N, 7.75; S, 17.75. Observed: C, 43.30; H, 3.87; N, 7.70; S, 17.78.

2.3. Synthesis of $Zn(dmpz)_2Cl_2$ (**3**)

0.136 g (2.0 mmol) $ZnCl_2$ in 5 mL dry methanol is added to the ethanolic solution of L^1 (1 mmol, 0.18 g) and reflux for 3 h where upon a white compound is obtained. Recrystallization of the crude product from acetonitrile produces good quality crystals of 4 suitable for X-ray crystallography. Yield: 78%. *Anal.* Calc. for $C_{10}H_{16}Cl_2N_4Zn$: C, 40.42; H, 5.65; N, 15.71. Observed: C, 40.35; H, 5.70; N, 15.75. IR/cm^{-1}: $\nu_{(C=N)}$ 1573, $\nu_{(C-N)}$ 1472. Mass spectrum *m*/*z* value: 354 (molecular ion peak).

2.4. Synthesis of $[Cd(dmpz)_2Cl_2]_n$(**4**)

0.209 g (1.0 mmol) $CdCl_2{\cdot}H_2O$ in 10 mL dry ethanol is added to the ethanolic solution of L^1 (2 mmol, 0.36 g) and reflux for 3 h where upon a bright yellow mass is obtained. Light yellow single crystals of **3** suitable for X-ray structure determination were obtained by the evaporation of aqueous ethanol (v/v 1:1) over a long period of time at room temperature. Yield 70%, *Anal.* Calc. for $C_{30}H_{48}Cd_3Cl_6N_{12}$: C, 33.18; H, 4.54; N, 13.27. Observed: C, 33.14; H, 4.52; N, 13.35. IR/cm^{-1}: $\nu_{(C=N)}$1585, $\nu_{(H2O)}$ 3417, $\nu_{(C-N)}$ 1405.

2.5. Characterization

The elemental analysis (C, H, N, and S) of the ligand and complexes were performed using FISONS EA-1108 CHN analyzer. Cyclic voltammetric experiments were performed at room temperature in methanol solvent using tetra butyl ammonium perchlorate as a supporting electrolyte on a CH Instrument electrochemical workstation model CHI630E. The conventional three-electrode assembly is comprised of a platinum working electrode, a platinum wire auxiliary electrode and a Ag/AgCl reference electrode. The IR spectra (4000–500 cm^{-1}) were recorded on a Perkin Elmer Spectrum Two FT-IR Spectrophotometer with sample prepare as KBr pellets. UV–Vis absorption spectra of the samples were recorded on a Perkin Elmer Lambda 35 spectrophotometer in the wavelength range region 200–800 nm at room temperature. Mass spectra of ligands were obtained using a Waters HRMS XEVO-G2QTOF#YCA351. All the quantum chemical calculations were performed using density functional theory (DFT) implemented in GAUSSIAN 09. The optimization was done using split basis set. The B3LYP hybrid functional and 6-31 g (d,p) basis set for hydrogen, carbon, nitrogen, sulfur and LANL2DZ basis set for copper are used for the optimization of all the geometries. The single crystal X-ray diffraction of **2**, **3** and **4** was carried out on a Bruker SMART APEX II X-ray diffractometer equipped with graphite-monochromated Mo Kα radiation (λ = 0.71073 Å) and 16 CCD area detector. The intensity data were collected in the π and ω scan mode, operating at 50 kV, 30 mA at 296 K [37]. The data reduction was performed using the SAINT and SADABS programs [38]. All calculations in the structural solution and refinement were performed using the Bruker SHELXTL program [39]. The structure was solved by the heavy atom method and refined by full-matrix least-squares methods. All the non-hydrogen atoms were refined anisotropically; the hydrogen atoms were geometrically positioned and fixed with isotropic thermal parameters. The final electron density maps showed no significant difference.

The catecholase activity of **1** and **2** was examined by the reaction of 100 equivalents of 3,5-di-*tert*-butylcatechol (3,5-DTBCH$_2$) with 1×10^{-5} M solutions of the complexes under aerobic conditions at ambient temperature in methanol. The reaction was followed spectro photometrically by monitoring growth of the absorbance as a function of time at *ca.* 400 nm which is characteristic of *o*-quinone chromophore. To determine the dependence of rate of the reaction on substrate concentration and to evaluate various kinetic parameters, 1×10^{-5} M solutions of the complexes were mixed with at least 10 equivalents of substrate to maintain pseudo-first order condition. To check the rate dependency on catalyst concentrations similar set of experiments were performed at a fixed concentration of substrate with various catalyst concentrations. The rate of a reaction was determined by the initial rate method, and the average initial rate over three independent measurements was recorded.

3. Result and discussion

3.1. Complex formation reaction

In an objective to develop a model system for mimicking catechol oxidase, coordination compounds derived from N(1) substituted 3,5-dimethylpyrazolyl (dmpz) ligands, e.g., L^1 and L^2 (Scheme 1) and d^{10} metals (e.g., Cu^I, Cd^{II} and Zn^{II}) were synthesized and structurally characterized. Extension of the ligand 3,5-dimethyl pyrazole (dmpz) in N(1) position with substitution –C(S)SR group (R = –Me or –CH_2Ph) imparts one additional bonding site (S) in the ligand which forms chelate changing significantly the coordination properties. In order to study the coordination properties of the pyrazolyl NS-donor ligands, L^1 and L^2 were reacted with $M^{II}Cl_2$ salts (M = Cu, Cd and Zn). Both chelates L^1 and L^2 act as neutral bidentate ligands with pyrazolyl ternary ring N(2) and thione S atom in $[Cu(L^1)_2][CuCl]$ (**1**) and $[Cu(L^2)_2][CuCl]$ (**2**). These sulfur containing ligands have sufficient reducing properties to reduce Cu^{II} to Cu^I in the reaction condition and attempts to prepare copper(II) chelates with L^1 and L^2 therefore result the formation of complexes **1** and **2**, respectively. The thermodynamic stability of these complex species resulted mainly from the chelate effect as the CFSE contribution is zero for Cu(I) (d^{10} system). Reduction of metal during complexation with sulfur containing N-heterocyclic chelate was also reported earlier though the reason is not clearly explained there [40].

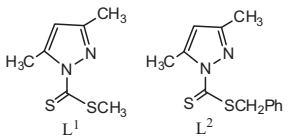

Scheme 1. Ligand structures.

Unlike reaction with $CuCl_2{\cdot}2H_2O$, we observe that the reactions of ligand L^1 and L^2 with other d^{10} species e.g., $ZnCl_2$ and $CdCl_2{\cdot}H_2O$, take place following a dissociation of the ligands into dmpz before the formation of corresponding complexes. A monomeric Zn(dmpz)$_2$Cl$_2$ (**3**) and a stable Cl-bridged polymer with composition $[Cd(dmpz)_2Cl_2]_n$ (**4**) were formed, respectively. The dissociation of L^1 and/or L^2 into parent ligand (dmpz) is attributed to the metal catalyzed dissociation leading to formation of basic ligand (dmpz) and O,O′-dialkyl ester of thiocarbonic acid with the evolution of RSH (alkyl thiol) for which a rational mechanism is proposed and shown in Scheme 2. Preparations of complexes with zinc(II) and cadmium(II) keeping the structural identity of L^1 and L^2 in the products were unsuccessful. The existence of dmpz in the coordination sphere reveals the dissociation of L^1 and/or L^2 into dmpz occurs is the presence of metal ion during complex formation. The reasons are by no means certain but no doubt involve several factors, of which size of the ligand is probably a major one. Being a smaller donor (N-donor) than ligand L^1 and/or L^2 (NS-donor), dmpz prefers to stabilized the bridged Cd(II)-dmpz complex than Cd(II) chelates with L^1 and L^2.There is a delicate balance between formation of chelate complex with undissociated ligand molecules (L^1/L^2) and formation of polymeric chain with dissociated fragment dmpz. High polymerization effect that includes the hydrogen bonding in the system outweighs the combined effects of chelate formation and ligand dissociation leading to formation of a relatively stable chain structure. The strong intermolecular interactions also give the thermodynamic stability of the Cl-bridged complex **4**.

On the other hand, $ZnCl_2{\cdot}6H_2O$ with L^1/L^2crystallizes as monomeric Zn(dmpz)$_2$Cl$_2$ (**3**). The presence of dmpz in the coordination sphere once again proves that the chelating ligand (L^1/L^2) has the tendency to dissociate into basic unit of pyrazole in presence of metal before crystallization into a stable product. Here also the chelate effect is not prominent in the non-transition Zn^{II} ion system. Since the d^{10} configuration (e.g., Zn^{II} and Cd^{II}) have no CFSE, then the stereochemistry of a particular compound depends on the size, polarizing power of M^{II} ions and the steric requirement of the ligand(s). The reason for the formation of monomeric Zn-complex instead of polymeric structure as in the case in $[Cd(dmpz)_2Cl_2]_n$ (**4**) may be attributed to the smaller size of Zn^{2+} (74 pm) than Cd^{2+} (95 pm). The smaller size of Zn(II) would have given much more strain to the bridged complex. In fact, in literature, the polymeric complexes of pyrazole based ligands with Cd^{2+} ion are numerous than Zn^{2+} ions [41]. Dissociation of substituted 3,5-dimethyl pyrazole ligand into dmpz is reported earlier in the literature [42,43]. 1-carboxamide-3,5-dimethyl pyrazole formed complexes with $CuCl_2$ and $CuCBr_2$ with a coordination to dissociated dmpz. It was supposed that Bronsted basicity of Cl

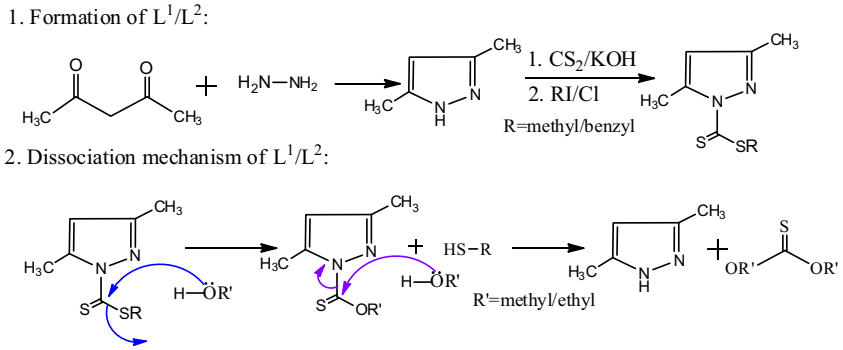

Scheme 2. Dissociation mechanism of ligand L^1 and L^2 to dmpz.

and Br ions low to promote the carboximide group for fair coordination. But the decarboxamidation of 1-carboxamide-3,5-dimethyl pyrazole to dmpz leads to formation of Cu-dmpz complex [44].

Free energy calculation for **3** and **4** (as proposed in the Scheme 2) give the values −39.67 and −32.84 kcal/mole, respectively (Table S1) attesting the dissociation of parent ligand into dmpz. It is also worth noting that the free energy value of the reaction of $CuCl_2$ and L^1 according to the proposed reaction scheme is −35.62 kcal/mol. However, the stabilization of $[Cu(L^1)_2][CuCl]$ (**1**) and $[Cu(L^2)_2][CuCl]$ (**2**) with retention of original ligand structure may be explained with strong chelate effect of the system with smaller copper ion than cadmium or zinc ion. It can be concluded that N^1 substituted 3,5-dimethyl pyrazolyl ligands having size larger than 3,5-dimethyl pyrazole (dmpz) have a tendency to dissociate into mono dentate dmpz with sufficient thermodynamic stability during coordination with relatively larger d^{10} ion until unless sufficient chelate effect come into force in the system.

3.2. Description of crystal structures

The structures of $[Cu^I(L^2)_2][Cu^ICl_2]$ (**2**), $Zn(dmpz)_2Cl_2$ (**3**) and $[Cd(dmpz)_2Cl_2]_n$ (**4**) have been determined by single crystal X-ray diffraction method. Structural characterization of the complex **1** is reported earlier by us [34]. To compare the structural features with isostructural complex **2**, the details of complex **1** (ORTEP and crystal data) is reproduced along with other complexes. The details of the refinement of all compounds reported are given in Table 1. The perspective views of molecular structures of **1** and **2** are depicted in Figs. 1 and 2, respectively, and the selected bond lengths and angles are given in Table 2. Both **1** and **2** crystallized in same fashion with similar geometry. The coordination geometry

Table 1
Crystal data and structure refinements for compounds **1**–**4**.

	1[*]	**2**	**3**	**4**
Formula	$C_{14}H_{20}Cl_2Cu_2N_4S_4$	$C_{26}H_{28}Cl_2Cu_2N_4S_4$	$C_{30}H_{48}Cd_3Cl_6N_{12}$	$C_{10}H_{16}Cl_2N_4Zn$
Mr	570.62	722.74	1126.70	328.56
Crystal system	triclinic	triclinic	triclinic	monoclinic
Space group	$P\bar{1}$	$P\bar{1}$	$P\bar{1}$	$C\,2/c$
T (K)	100	293	293	293
a (Å)	10.5271(9)	7.775(3)	9.5338(13)	15.0045(17)
b (Å)	10.7784(9)	12.790(4)	12.4107(17)	8.2983(7)
c (Å)	10.9396(9)	16.256(6)	20.436(3)	23.957(2)
α (°)	68.855(4)	71.425(11)	84.995(3)	90
β (°)	65.795(4)	86.823(11)	79.306(3)	95.790(4)
γ (°)	78.787(5)	81.026(12)	68.158(3)	90
V (Å^3), Z	2	2	2	8
D_{calc} (g cm^{-3})	1.797	1.586	1.697	1.471
Absorption coefficient (mm^{-1})	2.674	1.881	1.834	2.000
$F(000)$	576.0	736.0	1116.0	1344.0
$F(000')$	578.93	738.98	1113.14	1348.83
h, k, l (max)	14, 14, 14	9, 15, 19	11, 14, 24	17, 9, 28
R_1	0.0526(4419)	0.1143(2016)	0.0407(6503)	0.0285(2262)
wR_2	0.1420(5169)	0.3094(5028)	0.1078(7746)	0.0772(2612)
2θ(maximum)	56.60	49.44	50.00	50.00

[*] Ref. [34].

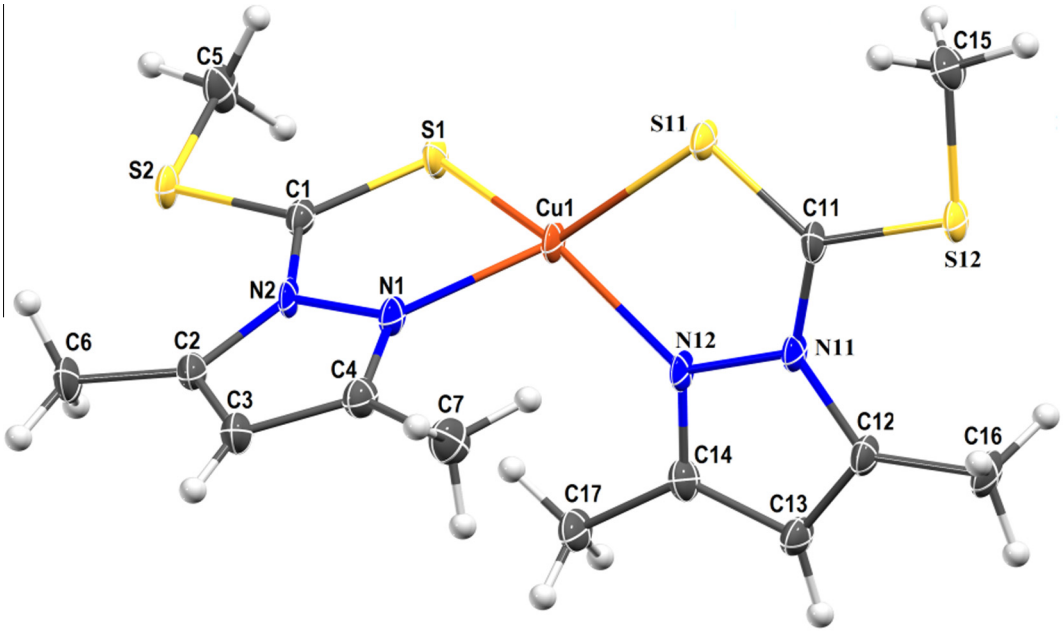

Fig. 1. Molecular structure of **1** showing the atom numbering scheme. Ellipsoids are drawn at the 30% probability level.

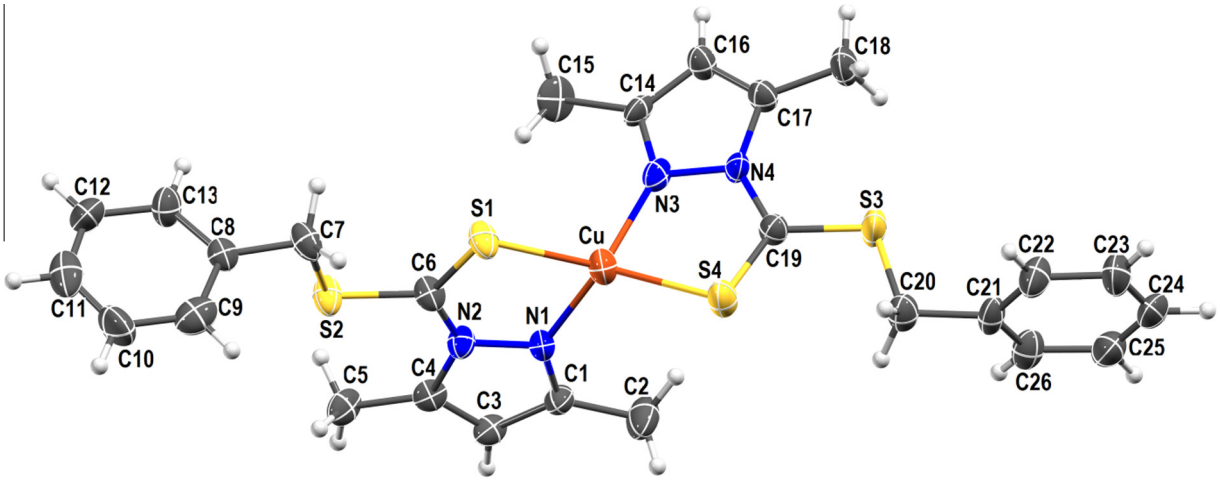

Fig. 2. Crystal structure of **2** showing the atom numbering scheme. Ellipsoids are drawn at the 30% probability level.

Table 2
Selected bond lengths (Å) and bond angles (°) of **1**–**4**.

1[*]		**2**		**3**		**4**	
Bond	Angle (°)	Bond	Angle (°)	Bond	Angle (°)	Bond	Angle (°)
S1–Cu1–N1	84.53(8)	S1–Cu1–S4	134.9(2)	N1–Zn1–N3	103.50(9)	Cl3–Cd1–Cl6	90.29(5)
S1–Cu1–S11	121.61(4)	S1–Cu1–N1	84.2(4)	N1–Zn1–Cl1	101.98(7)	Cl3–Cd1–Cl4	79.41(4)
S1–Cu1–N12	130.53(9)	S1–Cu1–N3	115.3(4)	N1–Zn1–Cl2	114.88(7)	Cl3–Cd1–Cl5	85.20(4)
N2–Cu1–S11	133.22(9)	S4–Cu1–N1	120.0(4)	N3–Zn1–Cl1	114.41(7)	Cl3–Cd1–N3	92.9(1)
N2–Cu1–N12	108.3(1)	S4–Cu1–N3	85.7(4)	N3–Zn1–Cl2	102.04(7)	Cl3–Cd1–N7	167.6(1)
S11–Cu1–N12	84.38(9)	N1–Cu1–N3	121.2(5)	Cl1–Zn1–Cl2	119.36(3)	Cl6–Cd1–Cl4	167.1(5)
Cu1–S1–C1	99.5(1)	Cu1–S1–C6	98.4(6)	Zn1–N1–N2	123.6(2)	Cl6–Cd1–Cl5	80.04(5)
C1–S2–C5	102.5(2)	Cu1–S4–C19	98.3(6)	Zn1–N1–C1	130.8(2)	Cl6–Cd1–N3	91.4(1)
N2–N1–C1	117.2(2)	Cu1–N1–N2	117.0(9)	N2–N1–C1	105.3(2)	Cl6–Cd1–N7	99.4(1)
N2–N1–C2	109.9(2)	Cu1–N1–C1	136(1)	Zn1–N3–N4	120.7(2)	Cl4–Cd1–Cl5	91.28(4)
C1–N1–C2	132.8(2)	Cu1–N1–N2	117.0(9)	Zn1–N3–C5	134.3(2)	Cl4–Cd1–N3	96.8(1)
Cu1–N2–N1	116.9(2)	Cu1–N1–C1	136(1)	N3–N4–H4	124.0	Cl4–Cd1–N7	89.9(1)
Cu1–N2–C4	135.6(2)	N2–N1–C1	107(1)	N3–N4–C7	112.1(2)	Cl5–Cd1–N3	171.2(1)
N1–N2–C4	106.2(3)	H3–C3–C1	126	H4–N4–C7	123.9	Cl5–Cd1–N7	88.8(1)
S1–C1–S2 l	122.9(2)	H3–C3–C4	126			N3–Cd1–N7	94.7(2)
Bond	Length (Å)	Bond	Length (Å)	Bond	Length (Å)	Bond	Length (Å)
Cu1–S1	2.2640	Cu1–S1	2.287	Zn1–N1	2.013	Cd1–Cl3	2.722
Cu1–N2	2.042	Cu1–S4	2.274	Zn1–N3	2.016	Cd1–Cl6	2.621
Cu1–S11	2.269	Cu1–N1	2.04	Zn1–Cl1	2.2259	Cd1–Cl4	2.638
Cu1–N12	2.025	Cu1–N3	2.01	Zn1–Cl2	2.2196	Cd1–Cl5	2.667
S1–C1	1.663	S1–C6	1.63	N1–N2	1.354	Cd1–N3	2.278
S2–C1	1.730	S2–C6	1.75	N1–C1	1.336	Cd1–N7	2.317
S2–C5	1.794	S2–C7	1.82	N3–N4	1.357	Cd2–Cl1	2.679
N1–N2	1.396	S3–C19	1.72	N3–C5	1.328	Cd2–Cl3	2.695
N1–C1	1.389	S3–C20	1.80	N4–H4 1	0.861	Cd2–Cl4	2.647
N1–C2	1.407	S4–C19	1.64	N4–C7	1.334	Cd2–Cl2	2.596

[*] Ref. [34].

of both the complexes around the Cu-atom is tetrahedral with an N_2S_2 chromophore with the participation of two ligand moieties. Cu(I) is coordinated by the ternary N-atom of pyrazole ring and thione sulfur of each ligand and a linear $Cu^{I}Cl_2$ unit is present outside the coordination sphere to satisfy the residual charge. In complex **1**, the chelate bite angle of N(1)–Cu(1)–S(1) and N(12)–Cu(1)–S(11) are 84.53(8)° and 84.38(9)°, respectively. The corresponding chelate bite angles in complex **2** i.e., N(1)–Cu(1)–S(1) and N(3)–Cu(1)–S(4) are 84.2(4)° and 85.7(4)°, respectively. These bite angles are much smaller than the ideal tetrahedral angle (109.28°) as well as the other two tetrahedral angles N(2)–Cu(1)–N(12) [108.3(10)°]and S(1)–Cu(1)–S(11) [121.61(3)°] in **1**, and S(1)–Cu(1)–N(3) [115.3(4)] and S(4)–Cu(1)–N(1) [120.0(4)] in **2**. The lowering of the biting angles is due to the closeness of the coordinating N and S atoms in the ligand with a view to facilitate the formation of 5-membered chelate rings. The angle N(2)–Cu(1)–N(12) [108.3(10)°] in **1** reveals that the out plane position of the two adjacent pyrazole rings giving less steric crowding among methyl groups at 3(5) position. In complex **2**, the pyrazole rings are also situated in out plane position to minimize the crowding in 3(5) position with angle N(1)–Cu(1)–N(3) [121.2(5)°].

$Zn(dmpz)_2Cl_2$ (**3**) crystallized in the monoclinic *C*2/*c* space group with all atoms in general positions and the whole molecule given by the formulae is present in the asymmetric unit (Fig. 3). In **3**, the coordination sphere around the Zn atom adopts a distorted tetrahedral environment. The coordination sphere consists of two nitrogen atoms of 3,5-dimethyl pyrazole (dmpz) and two chlorine atoms. The coordination angles vary in the range 101.98(7)–119.36(3). The Cl1–Zn1–Cl2 angle is very high [119.36(3)] from the idealized tetrahedral bond angle proving that the Cl–Cl crowding

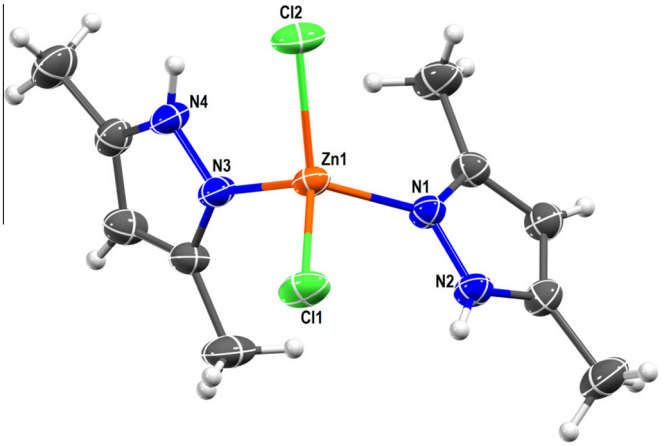

Fig. 3. Molecular structure of **3** showing the atom numbering scheme. Ellipsoids are drawn at the 30% probability level.

is relatively greater than the methyl–methyl repulsion in the dmpz. The two dmpz ring planes are nearly perpendicular with each other as suggested by the dihedral angle between two planes of 84.62°. Crystal packing of **3** is mainly stabilized by significantly strong hydrogen bonding interaction (Table 3) involving chloride ions and pyrazolyl protons of the adjacent molecules, leading to the formation of 1D supramolecular hydrogen bonded chain structure as shown in Fig. 4.

The crystal structures of **4** constructed 1D polymers consisting of doubly bridged metal centers with Cl atoms (Fig. 5). In the chains, Cd···Cd separation is found to be 4.111 Å. The six coordinated geometry of the complex **4** is somewhat distorted octahedron as reflected from the significant deviation of the *cisoid* and *transoid* angles from the ideal values. In addition to the four bridging Cl atoms, the coordination number of Cd is completed by the two neutral monodentate dmpz ligand which are *cis* coordinated. The axial positions are occupied by a bridging Cl atom and a ternary pyrazolyl nitrogen in **4**, with Cl3–Cd1–N7 angle of 167.6 (1)°. The adjacent Cd_2Cl_2 planes are almost perpendicular to each other in which dihedral angles between the adjacent Cd_2Cl_2 cores vary in the range 84.32–85.22°. Such an arrangement increases the possibility of the intra-chain hydrogen bonding interactions between bridging chlorides and pyrazole protons with donor-accepter distances in the range 3.140–3.189 Å (Table 2). Careful inspection of crystal packing further reveals that Cd and one bridging Cl construct a helical chain along the crystallographic *a*-axis and pitch of the helix is just equal to one unit cell length of the *a*-axis (9.5338(13) Å). However, two adjacent helices with alternating right- and left-handed chiralities are packed together along the *a*-axis leading to racemic helical polymers which is consistent with the centro symmetric space group $P\bar{1}$ in the triclinic unit cell. Another interesting feature of compound **4** is that similar homochiral chains are stacked along the *b*-axis (Fig. 6) with the helix-to-helix separation of 12.4107(17) Å, which is equal to the length of the *b*-axis. Therefore, the features of the chain structures in the complex arise from the intra molecular hydrogen bonding interactions; pyrazolyl ligand able to participate in hydrogen bonding interaction with bridging chlorides there by induce helicity in the chain structure in **4**. The present example clearly justifies that the non-covalent interactions like hydrogen-bonding is involved to stabilize folded protein like structures instead of linear chain in the biological systems.

Table 3
Hydrogen bond parameters (Å, °) for **3** and **4**.

Complex	D–H···A	*d*(D–H)	*d*(H···A)	*d*(D···A)	<D–H···A
3	N4–H4···Cl2[a]	0.86	2.82	3.329(3)	128
	N2–H5···Cl1[a]	0.86	2.66	3.475(2)	160
4	N8–H8···Cl1[b]	0.86	2.35	3.175(5)	160
	N9–H9···Cl5[c]	0.86	2.33	3.163(5)	165
	N10–H13···Cl1	0.86	2.33	3.159(5)	162
	N11–H5···Cl3[c]	0.86	2.36	3.206(5)	167
	N12–H20···Cl3	0.86	2.36	3.189(5)	161
	N15–H4···Cl5	0.86	2.32	3.140(5)	160

Symmetry code: a = 2 − *x*, *y*. 3/2 − *z*; b = 1 + *x*, *y*, *z*; *c* = −1 + *x*, *y*, *z*.

3.3. Electrochemical studies of *1* and *2*

The experiment were performed to assess the redox behavior of complex **1** and **2** in solution in order to check the feasibility of catecholase activity of the relevant synthesized species. In the biological systems, redox potential of metallo-enzymes plays crucial role for redox transformation in the biochemical reactions. The studies of the electrochemical behaviors of the complexes have been performed in the identical experimental conditions as that of kinetic studies (vide infra). The electrochemical data of the complex **1** and **2** have been recorded in methanol in presence of tetra butyl ammonium perchlorate (0.1 M) as a supporting electrolyte at a platinum working electrode and using a Ag/AgCl reference electrode. Electrochemical responses of both complexes are similar and cyclic voltammograms of **1** and **2** are depicted in Fig. 7. Scanning in the anodic direction reveals an oxidative response at 0.50 V for **1** and 0.47 V for **2** versus Ag/AgCl electrode. Upon reversal of scan direction a reduction process is appeared at 0.33 V for **1** and

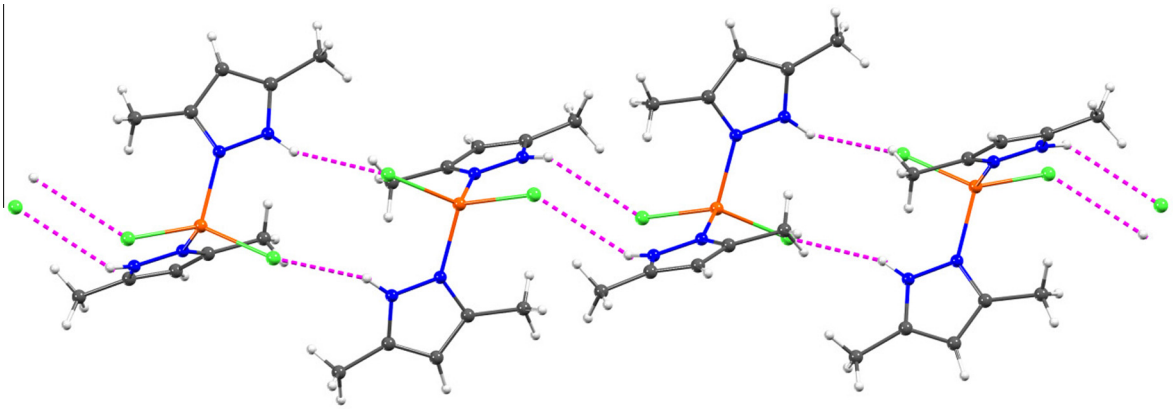

Fig. 4. 1D hydrogen bonded supramolecular chain of **3**.

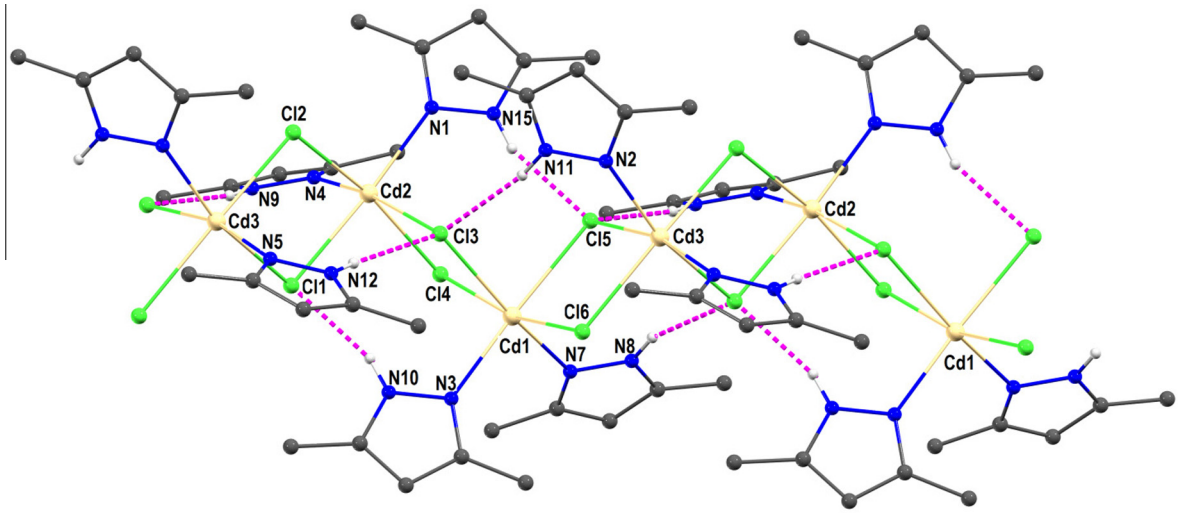

Fig. 5. Double chloride-bridged cadmium polymer of **4** showing intramolecular hydrogen bonding interactions.

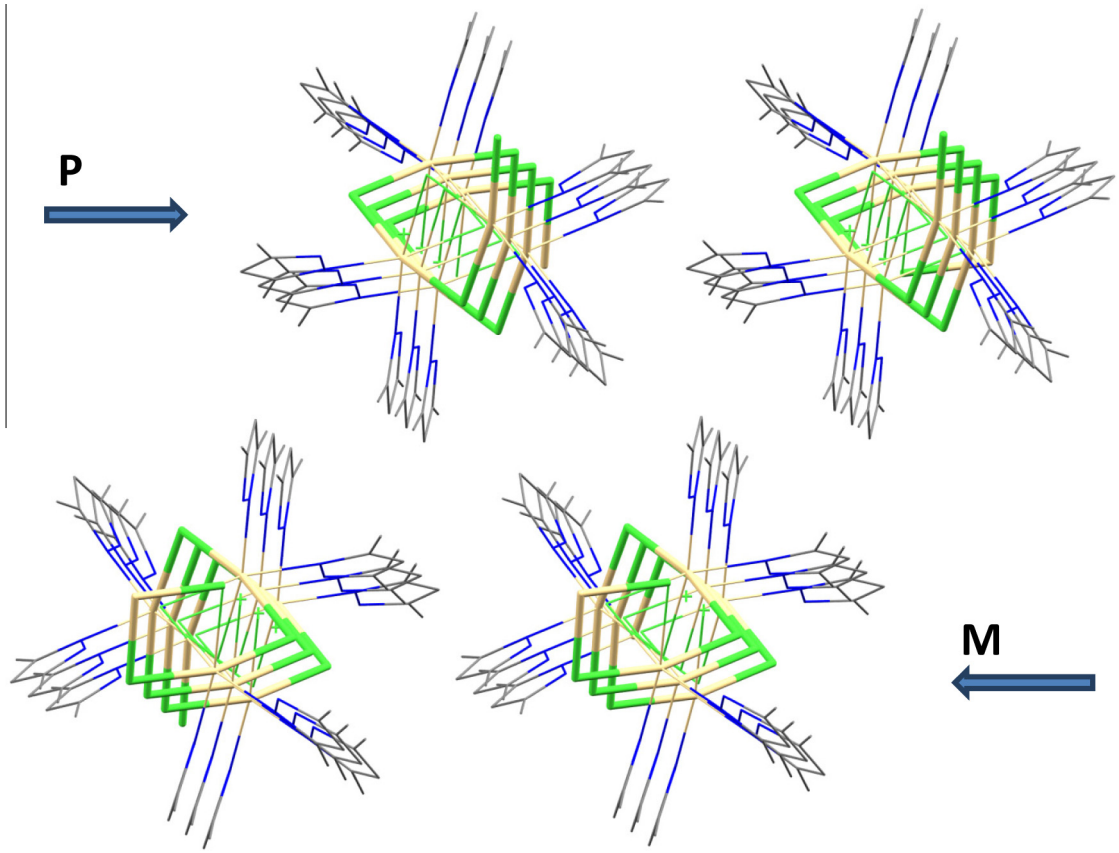

Fig. 6. Molecular packing of **4**, viewed along the *a*-axis, showing the alternating stack of left and right-handed helices propagated along the *b* axis.

0.32 V for **2**. These quasi reversible redox processes are responsible for copper(II)/copper(I) redox couple. From the electrochemical data (ΔE_p = 0.17 V, $E_{1/2} = (E_{pa} + E_{pc})/2$ = 0.42 for **1** and ΔE_p = 0.15 V, $E_{1/2}$ = 0.40 for **2**), it is clear that the electrochemical responses of both complexes are very similar which is consistent with both identical geometry and coordination environment around the metal center. Slightly different electrode potentials may be due to the effect of substitution at the ligand backbone along with different extent of geometrical distortion present in the complexes.

3.4. Catechol oxidase mimetic activity

Catechol oxidase is a dinuclear copper enzyme that catalyzes the two electron transfer reaction during the oxidation of a wide range of catechols to the corresponding *o*-quinones by O_2. We introduced analogous Cu(I)-pyrazolyl complexes (**1** and **2**) to check the catecholase activity in this report. Catecholase activity is usually studied with 3,5-di-*tert*-butylcatechol (3,5-DTBC) as substrate because of its lower redox potential that facilitates ease of

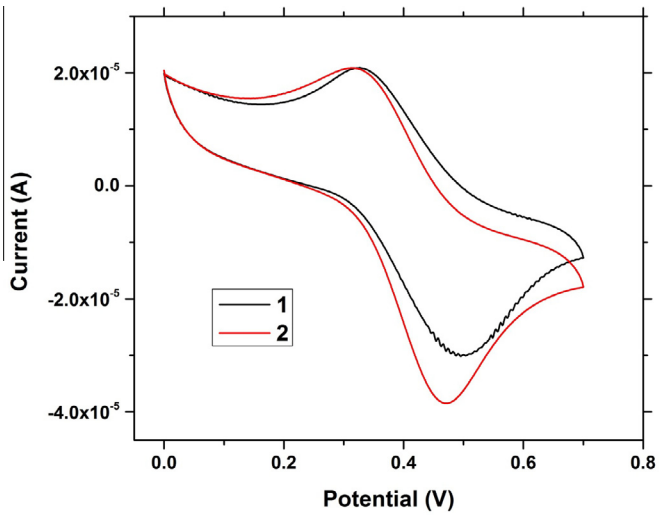

Fig. 7. Cyclic voltammograms of **1** and **2** in methanol solution using a platinum working electrode in the presence of tetra butyl ammonium perchlorate as a supporting electrolyte at ambient temperature with scan rate 100 mV s^{-1}.

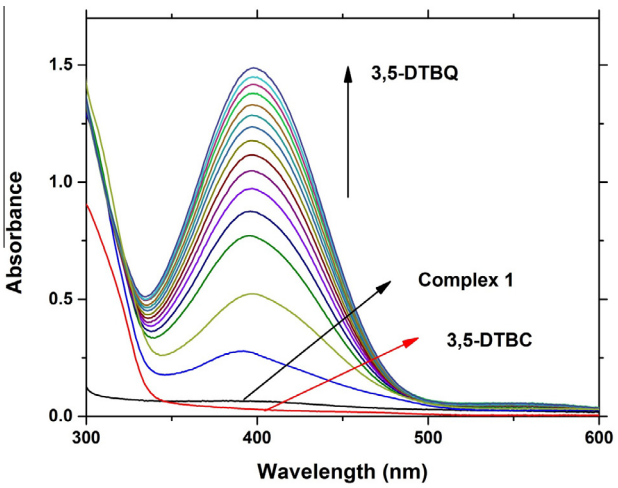

Fig. 8. The spectral profile showing growth of 3,5-DTBQ at 400 nm upon addition of 0.001 M 3,5-DTBQ to a solution containing **1** (1×10^{-5} M) in methanol. The spectra were recorded in 5 min time interval for a cumulative time period of 1 h in aerobic condition at room temperature.

oxidation of 3,5-DTBC and the bulky substituents prevent further reactions such as ring-opening process. The product 3,5-di-*tert*-butyl-*o*-quinone (3,5-DTBQ) is quite stable in air and has a characteristic transition at about 400 nm and therefore catalytic study can be monitored by UV–Vis spectrophotometry. Reactivity and kinetic studies were performed in methanol because of the good solubility of the complexes, substrate and their product in this solvent. Before going to the detailed kinetic investigation, it is first necessary to check the ability of the complexes to behave as catalysts for the catechol oxidase mimetic activity. Accordingly, 1.0×10^{-5} M solutions of the complexes were treated with 200-fold concentrated solution of 3,5-DTBC, and the spectra were recorded up to 1 h in dioxygen saturated methanol at room temperature. The time dependent spectral changes for a period of 1 h after the addition of 3,5-DTBC are displayed in Figs. 8 and 9 for **1** and **2**, respectively. The spectral scan reveals the increase of the band intensity at *ca.* 400 nm characteristic of quinone chromophore for both complexes although a blank experiment using copper chloride salt instead of the complexes did not show signif-

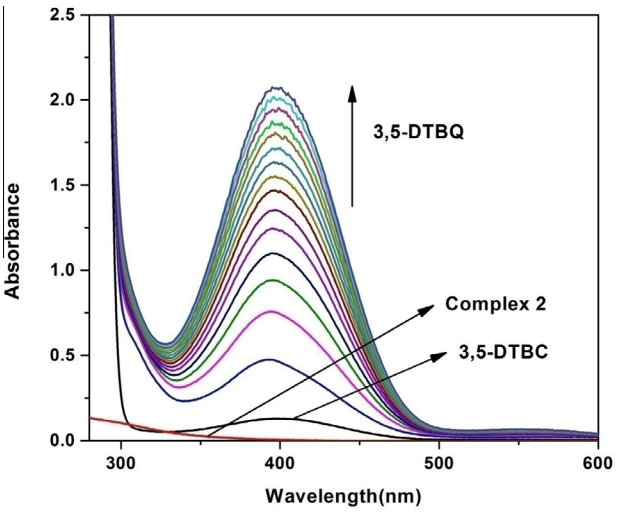

Fig. 9. The spectral profile showing growth of 3,5-DTBQ at 400 nm upon addition of 0.001 M 3,5-DTBQ to a solution containing **2** (1×10^{-5} M) in methanol. The spectra were recorded in 5 min time interval for a cumulative time period of 1 h in aerobic condition at room temperature.

icant spectral growth. These results suggest that **1** and **2** are active towards the catecholase activity.

Kinetic studies were performed to understand the extent of the catalytic efficiency of both complexes, and for this purpose 2×10^{-5} M solutions of the complexes were mixed with at least 10-fold concentrated substrate solution to follow the pseudo-first-order condition. For a particular complex-substrate mixture, time scan at the maximum of quinone band was carried out for a period of 10 min, and the initial rate was determined by linear regression from slope of the absorbance versus time. The initial rate of reactions versus concentration of the substrate data show a first-order rate dependence on the substrate concentration at lower concentrations of 3,5-DTBC but almost zero order at the higher concentrations (Fig. 10). This observation suggests that quinone formation proceeds through a relatively stable intermediate, a complex–substrate adduct, followed by the irreversible redox

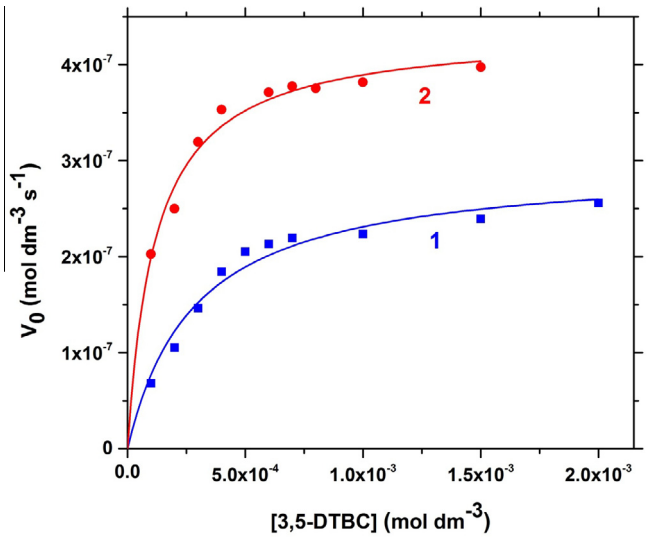

Fig. 10. Initial rate versus substrate concentration plot for the oxidation of 3,5-DTBC in air-saturated methanol catalyzed by the complexes at room temperature. Symbols and solid lines represent the experimental and simulated profiles, respectively.

transformation of the intermediate at the rate determining step. This type of rate saturation kinetics on the concentration of the substrate may be explained by considering the Michaelis–Menten model, originally developed for the enzyme kinetics, which gives linear double reciprocal Lineweaver–Burk plot to analyze values of the parameters V_{max}, K_M, and K_{cat}. The observed and simulated initial rates versus substrate concentration plot and the Lineweaver–Burk plot for both complexes are shown in Fig. 11. Analysis of the experimental data yielded Michaelis binding constant (K_M) values of 2.84 (±0.38) × 10^{-4} M for **1** and 1.18 (±0.12) × 10^{-4} for **2** and V_{max} values of 2.97 (±0.12) × 10^{-7} M s^{-1} and 4.35 (±0.09) × 10^{-7} M s^{-1} for **1** and **2**, respectively. The turnover number (K_{cat}) value is obtained by dividing the V_{max} by the concentration of the catalyst used, and is found to be 106.9 and 156.6 h^{-1} for **1** and **2**, respectively. Moreover, for a particular substrate concentration, varying the complex concentration, a first-order dependency on the catalyst concentration was observed. The turnover rates are slightly higher than other copper(I) model systems and even also higher than some copper(II) model complexes [17], but significantly lower than those recently reported for the binuclear copper complexes found in the recent review on catechol oxidase model systems [45].

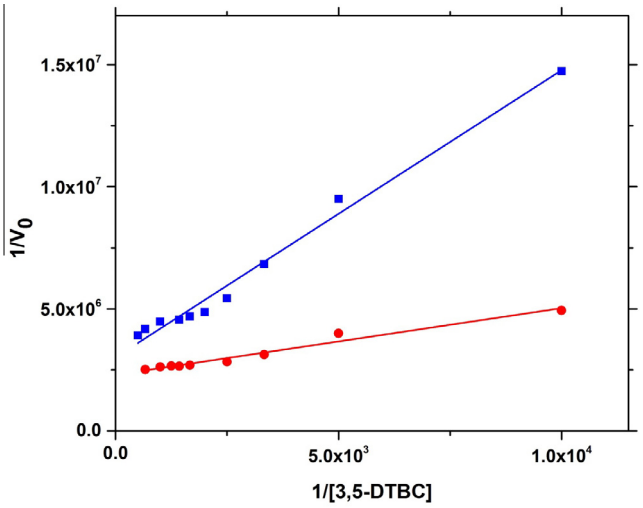

Fig. 11. Lineweaver–Burk plots for the oxidation of 3,5-DTBC catalyzed by **1** and **2** in methanol. Symbols and solid lines represent the experimental and simulated profiles, respectively.

3.5. Electrospray ionization mass spectral study

As both **1** and **2** have similar structural features, the electrospray ionization mass spectrum (ESI-MS positive) of the more reactive representative compound **2** was recorded in methanol solution and is shown in Fig. S1. The base peak at *m/z* = 325.05 with line-to-line separation of unity is assigned to $[Cu^{I}(L^{2})]^{+}$ (calculated *m/z* = 324.99). The peak at *m/z* = 587.12 with line-to-line separation of 1.0 is consistent with the whole molecular species of formula $[Cu^{I}(L^{2})_2]^{+}$ (calculated *m/z* = 587.05). In order to get further insight into the nature of possible complex–substrate intermediates, ESI-MS positive spectrum of a mixture of complex **2** and 3,5-DTBC in 1:50 molar ratio was recorded after 5 min of mixing in methanol. The observed spectrum as depicted in Fig. 12 is significantly different from the mass spectrum of complex **2** alone. As can be seen from the Fig. 12, the most abundant species found at *m/z* = 325.06 in the mass spectrum corresponds to the original compound **2** which is assigned to the mass of $[Cu^{I}(L^{2})]^{+}$. Another peak at *m/z* = 587.10 is again found in the mass spectrum of original compound which corresponds to the undissociated cationic

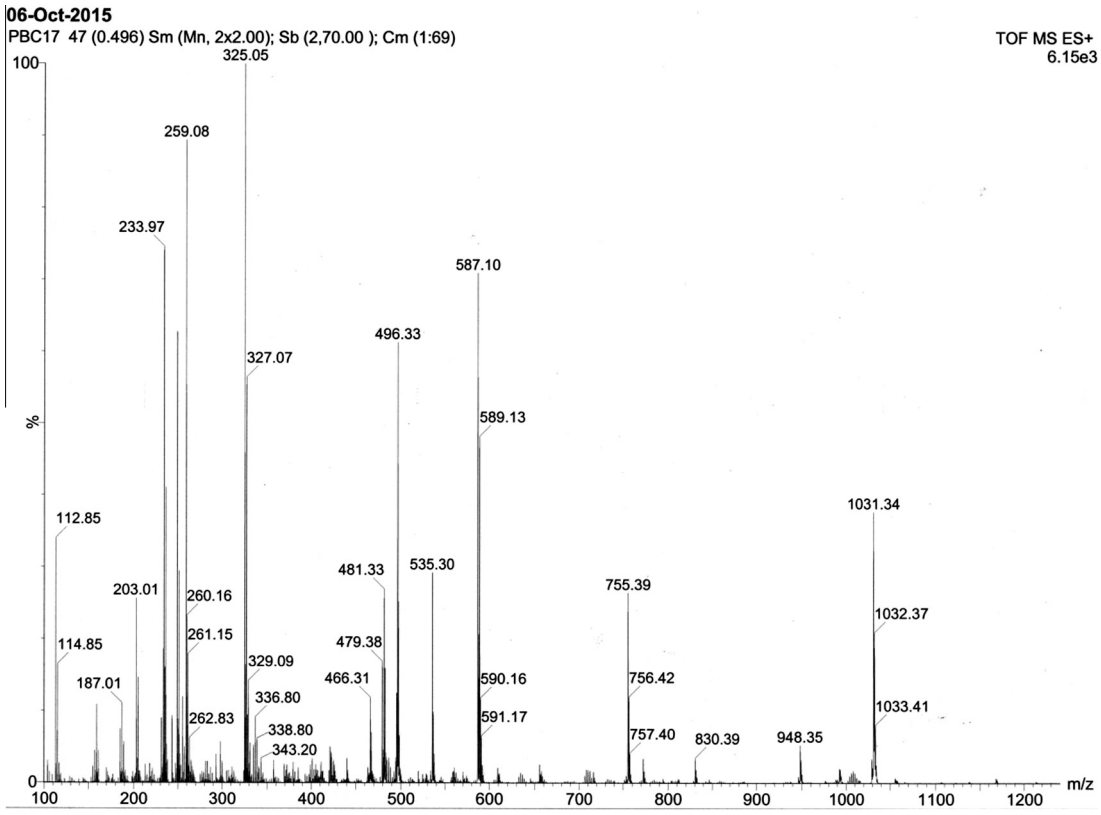

Fig. 12. Electrospray ionization mass spectrum (ESI-MS positive) of a 1:50 mixture of **2** and 3,5-$DTBCH_2$ in methanol, recorded after 5 min of mixing.

part of **2** i.e., $[Cu^{I}(L^{2})_2]^+$. In addition to the masses related to the original complex species, the mass at $m/z = 259.08$ is assignable to potassium adduct of product 3,5-DTBQ of unipositive species $[K + 3,5\text{-DTBQ}]^+$ (calculated $m/z = 259.11$). Another product related peak is found at $m/z = 755.39$ which can be assigned as a monocationic species of formula $[Na(3,5\text{-DTBQ})_3 + 4H_2O]^+$ (calculated $m/z = 755.47$). Most importantly, the peak at $m/z = 1031.34$ is quite interesting because the peak position and line-to-line separation of unity clearly indicate that the peak arises from the complex-substrate aggregate of unipositive species $[Cu^{I}(L^{2})_2\text{-}(3,5\text{-DTBC})_2]^+$ (calculated $m/z = 1031.37$). Another minor peak at $m/z = 655.09$ (Fig. S2) is also need to mention as that matches with dioxygen containing species of unipositive charge of formula $[Cu^{I}(L^{2})_2 + O_2 + 2H_2O]^+$ (calculated $m/z = 655.06$) although the same peak is much more prominent in the mass spectrum of the complex alone (found at $m/z = 655.09$) (Fig. S1).

3.6. Comparative catecholase activity and proposed mechanism

The reaction kinetics shows that both complexes are very reactive towards the catechol oxidase mimicking activity, and the rate saturation kinetics clearly indicates that the reaction proceeds through a stable complex substrate intermediate formation. The existence of $[Cu^{I}(L^{2})_2\text{-}(3,5\text{-DTBC})_2]^+$ species in mass spectrum of **2** in presence of excess 3,5-DTBC strongly supports the affinity of the complex cation towards the incoming substrate. Although mass spectroscopy does not necessarily reflect the actual species present in the solution state because some stable aggregates may be formed *in situ* (because of their relative stability) when compared to the other cationic species on the time scale of the ESI-MS spectrum. Nevertheless, the aggregates found in the ESI-MS spectra deserve importance because they offer clear evidence of coordination of the substrate to the complexes. In the mass spectrum, it can be noticed that m/z peak for the adduct of metal complex with the bulky benzyl substitution in **2** compared to methyl group in **1** does not inhibit the coordination of substrate to metal center. Therefore, the difference in catecholase activity between **1** and **2** can be explained by the redox potential of the metal centers in these systems-the ease of conversion of Cu(I) to Cu(II) in **2** (as suggested by the electrochemical data) favors the oxidation of 3,5-DTBC which is reflected from the higher K_{cat} value for **2**.

In order to justify the involvement of molecular dioxygen in the catalytic cycle, UV–Vis spectra of a mixture of 1×10^{-5} M solution of complex **1** with 100 fold excess of 3,5-DTBC were recorded in nitrogen atmosphere, and no spectral growth at 400 nm was observed. But upon exposure to air gradual increase of quinone band intensity at 400 nm is noticed. This observation unambiguously proves that molecular dioxygen oxidizes 3,5-DTBC to the corresponding 3,5-DTBQ in the catalytic cycle in the presence of copper(I) complex as a catalyst. In our recent study, we proposed that catecholate bound copper(I) complex react with molecular dioxygen to form a superoxo intermediate in which copper(I) center is oxidized to copper(II) [18]. The intermediate involved in the intramolecular proton transfer process from oxygen atom of catechol moiety to the superoxide oxygen atom is associated with electron transfer from catecholate to superoxide, leading to the formation of peroxo-intermediate at the rate determining step. That mechanistic pathway for the oxidation of catechol by molecular dioxygen was further supported by means of DFT study [18]. In the present system, mass spectral data suggests the interaction of both molecular dioxygen and substrate to the metal centers and thus one can expect that the catalytic oxidation of 3,5-DTBC may proceed thorough the similar mechanistic pathway [18]. It is noteworthy that if the rate determining step involves in breaking of the –O–H bond, a kinetic isotope effect (KIE) should be observed upon changing the solvent from CH_3OH to CH_3OD. In order to probe such mechanistic pathway, comparative kinetic studies were performed under a given set of conditions both in methanol and deuterated methanol, and the results indicate that about 1.9 times rate retardation is observed when the kinetic study is conducted in CH_3OD. Based on the above results, a plausible mechanism is tempted involving stepwise pathways, keeping in mind that it is impossible to prove any single mechanism (Scheme 3). The catalytic cycle is expected to start with the formation of complex–substrate aggregate which in turn produces the superoxide intermediate by the reaction with aerial oxygen in which copper(I) center undergoes an oxidation to a copper(II). The next step in the catalytic cycle is the rate determining one which involves the intramolecular proton transfer process from oxygen atom of catechol moiety to the

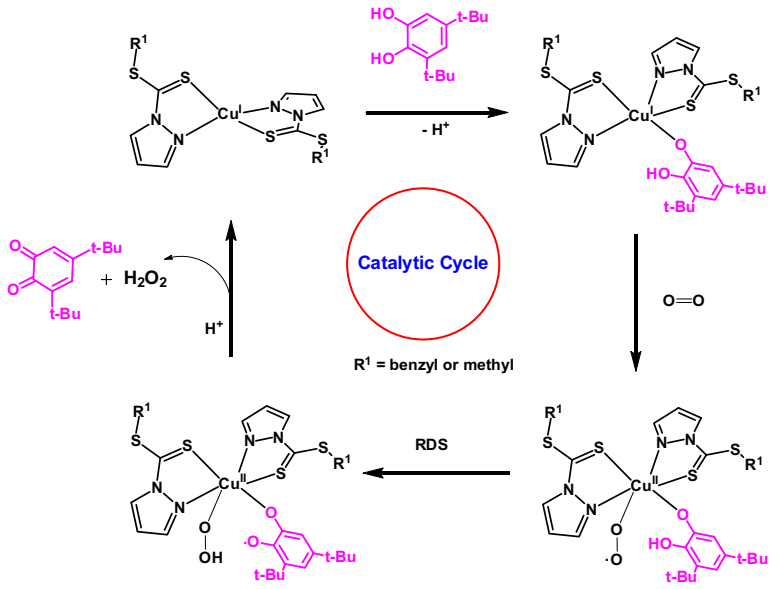

Scheme 3. Plausible mechanistic pathway for the oxidation of 3,5-DTBC by dioxygenin presence of catalyst **1** or **2**.

superoxide along with the intra molecular electron transfer to generate a peroxo-intermediate. Finally, the last step involves the rapid breakdown of the peroxo-intermediate to the products (3,5-DTBQ and H_2O_2) with concomitant regeneration of the active catalyst to complete the catalytic cycle.

4. Conclusion

Ligational behavior of 3,5-dimethyl pyrazole (dmpz) derived ligands (L^1 and L^2) were compared with d^{10} system e.g., Zn(II), Cd(II) and Cu(I). L^1 and L^2 behave as neutral bidentate NS chelate and stabilized the Cu(I) complex with composition $[Cu^I(L^1/L^2)_2][Cu^ICl_2]$ (**1** for L^1 and **2** for L^2). Whereas L^1 and L^2 dissociate into basic 3,5-dimethyl pyrazole before formation of monomeric Zn $(dmpz)_2Cl_2$ (**3**) and polymeric $[Cd(dmpz)_2Cl_2]_n$ (**4**) from the reaction of L^1 with $ZnCl_2$ and $CdCl_2$, respectively. Structural diversity of the d^{10} metal system with pyrazolyl ligands is attributed to the steric profile of the ligands. The most distinguished feature of bis(chloro) bridged chain structure of **4** arises from the intramolecular hydrogen bonding interactions. Pyrazolyl ligands able to participate in hydrogen bonding interaction with bridging chlorides thereby induce helicity in the chain structure in **4**. Copper analogues (**1** and **2**) exhibits efficient catecholase activity in which a nice correlation, the easily oxidizable copper(I) center favoring the oxidation of 3,5-DTBC is observed. The kinetics study exhibited a deuterium kinetic isotope effect in the catalytic oxidation of 3,5-DTBC by O_2, suggesting the hydrogen atom transfer in the rate-determining step from the substrate hydroxy group to the metal-bound superoxo species. Thus copper(I) complexes with pyrazolyl NS chelate with sufficient stability may thus be a classic example in mimicking copper catalytic reactivity and need to be explored further.

Acknowledgements

We gratefully acknowledge to the University Grants Commission (UGC), Government of India for financial support [Ref. Grant No. F 42-280/2013(SR)]. We are also thankful to Dr. Sang Il Seok of Korea Research Institute of Chemical Technology (KRICT), South Korea for X-ray crystallographic data collection.

Appendix A. Supplementary data

CCDC 1431421–1431423 contains the supplementary crystallographic data for **2**–**4**. These data can be obtained free of charge via http://www.ccdc.cam.ac.uk/conts/retrieving.html, or from the Cambridge Crystallographic Data Centre, 12 Union Road, Cambridge CB2 1EZ, UK; fax: (+44) 1223-336-033; or e-mail: deposit@ccdc.cam.ac.uk. Supplementary data associated with this article can be found, in the online version, at http://dx.doi.org/10.1016/j.poly.2016.03.055.

References

[1] N.A. Rey, A. Neves, A.J. Bortoluzzi, C.T. Pich, H. Terenzi, Inorg. Chem. 46 (2007) 348.
[2] C. Belle, C. Beguin, I. Gautier-Luneau, S. Hamman, C. Philouze, J.L. Pierre, F. Thomas, S. Torelli, Inorg. Chem. 41 (2002) 479.
[3] J. Ackermann, F. Meyer, E. Kaifer, H. Pritzkow, Chem. Eur. J. 8 (2002) 247.
[4] M. Merkel, N. Mçller, M. Piacenza, S. Grimme, A. Rompel, B. Krebs, Chem. Eur. J. 11 (2005) 1201.
[5] A. Majumder, S. Goswami, S.R. Batten, M.S. El Fallah, J. Ribas, S. Mitra, Inorg. Chim. Acta 359 (2006) 2375.
[6] M.K. Panda, M.M. Shaikh, R.J. Butcher, P. Ghosh, Inorg. Chim. Acta 372 (2011) 145.
[7] A. Panja, S. Goswami, N. Shaikh, P. Roy, M. Manassero, R.J. Butcher, P. Banerjee, Polyhedron 24 (2005) 2921.
[8] S. Majumder, S. Sarkar, S. Sasmal, E.C. Sañudo, S. Mohanta, Inorg. Chem. 50 (2011) 7540.
[9] S.Y. Shaban, A.E.-M.M. Ramadan, M.M. Ibrahim, M.A. Mohamed, R.V. Eldik, Dalton Trans. 44 (2015) 14110.
[10] Y. Thio, X. Yang, J.J. Vittal, Dalton Trans. 43 (2014) 3545.
[11] M.R. Mendoza-Quijano, G. Ferrer-Sueta, M. Flores-Álamo, N. Aliaga-Alcalde, V. Gómez-Vidales, V.M. Ugalde-Saldívar, L. Gasque, Dalton Trans. 41 (2012) 4985.
[12] M.J. Gajewska, W.-M. Ching, Y.-S. Wen, C.-H. Hung, Dalton Trans. 43 (2014) 14726.
[13] P. Comba, B. Martin, A. Muruganantham, J. Straub, Inorg. Chem. 51 (2012) 9214.
[14] K.S. Banu, T. Chattopadhyay, A. Banerjee, S. Bhattacharya, E. Suresh, M. Nethaji, E. Zangrando, D. Das, Inorg. Chem. 47 (2008) 7083.
[15] M. Rolff, J. Schottenheim, H. Decker, F. Tuczek, Chem. Soc. Rev. 40 (2011) 4077.
[16] G. Grigoropoulou, K.C. Christoforidis, M. Louloudiand, Y. Deligiannakis, Langmuir 23 (2007) 10407.
[17] Á. Kupán, J. Kaizer, G. Speier, M. Giorgi, M. Réglier, F. Pollreisz, J. Inorg. Biochem. 103 (2009) 389.
[18] M. Shyamal, T.K. Mandal, A. Panja, A. Saha, RSC Adv. 4 (2014) 53520.
[19] M.A. Halcrow, Dalton Trans. (2009) 2059.
[20] R. Mukherjee, Coord. Chem. Rev. 203 (2000) 151.
[21] J. Pérez, L. Riera, Eur. J. Inorg. Chem. (2009) 4913.
[22] M.G. Cowan, S. Brooker, Coord. Chem. Rev. 256 (2012) 2944.
[23] T.P. Camergo, F.F. Maia, C. Chaves, B. Souza, A.J. Bortoluzzi, N. Castilho, T. Bortotto, H. Terenzi, E.E. Castellano, W. Haase, Z. Tomkowicz, R.A. Peralta, A. Neves, J. Inorg. Biochem. 146 (2015) 77.
[24] M. Fontecave, J.L. Pierre, Coord. Chem. Rev. 170 (1998) 125.
[25] E.A. Lewis, W.B. Tolman, Chem. Rev. 104 (2004) 1047.
[26] K.A. Magnus, H. Ton, J.E. Carpenter, Chem. Rev. 94 (1994) 727.
[27] H. Sigel, Metal Ions in Proteins, Marcel Dekker, New York, 1981.
[28] T. Klabunde, C. Eicken, J.C. Sacchettini, B. Krebs, Nat. Struct. Biol. 5 (1998) 1084.
[29] A. Koval, P. Gamez, C. Belle, K. Selmeczi, J. Reedijk, Chem. Soc. Rev. 35 (2006) 814.
[30] K. Selmeczi, M. Reglier, M. Giorgi, G. Speier, Coord. Chem. Rev. 245 (2003) 191.
[31] R. Than, A.A. Feldmann, B. Krebs, Coord. Chem. Rev. 182 (1999) 211.
[32] B.J. Dervall, Nature 189 (1961) 311.
[33] A. Rompel, H. Fischer, D. Meiwes, K. Büldt-Karentzopoulos, R. Dillinger, F. Tuczek, H. Witzel, B. Krebs, J. Biol. Inorg. Chem. 4 (1999) 56.
[34] G. Mondal, P. Bera, A. Santra, S. Jana, T.N. Mandal, A. Mondal, S.I. Seok, P. Bera, New J. Chem. 38 (2014) 4774.
[35] F. de Sousa Gerimário, C. Gatto Claudia, S. RescklnÊs, M. Deflon Victor, J. Chem. Crystallogr. 41 (2011) 401.
[36] P. Bera, I.C. Baek, S.I. Seok, N. Saha, Russ. J. Coord. Chem. 35 (2009) 526.
[37] Bruker, SMART (Version 5.625) Data Collection Program, Bruker AXS Inc., Madison, Wisconsin, USA, 2001.
[38] Bruker, SAINT (Version 6.28a) and SADABS (Version 2.03) Data Reduction and Absorption Correction Program, Bruker AXS Inc., Madison, Wisconsin, USA, 2001.
[39] G.M. Sheldrick, SHELXTL (Version 6.12) Structure Analysis Program, Bruker AXS Inc., Madison, Wisconsin, USA, 2001.
[40] T.N. Mandal, S. Roy, A.K. Barik, S. Gupta, R.J. Butcher, S.K. Kar, Inorg. Chim. Acta 362 (2009) 1315.
[41] W.G. Haanstra, W.L. Driessen, R.A.G. Graff, J. Reedijk, Y.F. Wang, C.H. Stam, Inorg. Chim. Acta 186 (1991) 215.
[42] I.R. Evans, K.M. Szécsényi, V.M. Leovac, Acta Crystallogr., Sect. E 61 (2005) m641.
[43] B. Hollo, Z.D. Tomic, P. Pogany, A. Kovacs, V.M. Leovaca, K.M. Szecsenyi, Polyhedron 28 (2009) 3881.
[44] K.M. Szécsényi, V.M. Leovac, V.I. Češljević, A. Kovács, G. Pokol, G. Argay, A. Kálmán, G.A. Bogdanović, Ž.K. Jaćimović, A.S. de Biré, Inorg. Chim. Acta 353 (2003) 253.
[45] S.K. Dey, A. Mukherjee, Coord. Chem. Rev. 310 (2016) 80.